Comparison of Atmospheric Delay Statistics from Deep Space Network Arrays and nearby Site Test Interferometers

David D. Morabito, Larry D'Addario, and Susan G. Finley

Jet Propulsion Laboratory

California Institute of Technology

Pasadena, California 91109

USA

Phone: 818-354-2424, Fax: 818-394-6825, E-mail: David.D.Morabito@jpl.nasa.gov

Phone: 818-393-0389, Fax: 818-393-2488, E-mail: ldaddario@jpl.nasa.gov

Phone: 818-354-5669, Fax: 818-393-2488, E-mail: Susan.G.FInley@jpl.nasa.gov

Abstract

Several techniques have been explored and demonstrated that allow for greater data return on space-to-ground links. Among these techniques, arraying several smaller diameter dish antennas together is one method used in several arenas. These arrays can achieve larger effective area and gain than are available from a single larger antenna. This technique is routinely used by the NASA Deep Space Network (DSN) at 8.4 GHz where the incoming signals are much weaker than those experienced by the near-Earth satellite community. When considering arraying at much higher frequencies such as 32 GHz deep-space Ka-band, the phase alignment of the individual antenna signals is significantly disrupted by atmospheric turbulence. Since 2012, several downlink array demonstrations have been conducted using 32 GHz carrier signals emitted by the deep space probes Cassini and Kepler.

Site test interferometers (STIs) that receive signals from geostationary satellites have been deployed at all three DSN tracking complexes for long-term monitoring of atmospheric delay fluctuations. In a previous DSN array demonstration study involving the Cassini spacecraft, it was shown that statistics of the adjusted STI phase fluctuations matched the statistics of concurrent array demonstration phase fluctuations. These adjustments accounted for differences in antenna separation, elevation angle and spacecraft frequencies. The STI antenna separations were about 200 m and the DSN antenna separations were about 300 m. These adjustments made use of the thick-layer turbulence model that was applicable to the Goldstone desert climate during the summer months for which the data were acquired.

In this paper, we report on the results of additional array demonstrations involving the Kepler spacecraft and compare the adjusted STI phase fluctuations with those seen by a nearby two-element array of 34 m diameter antennas tracking Kepler's 32 GHz signal at the Goldstone, California and Madrid, Spain DSN sites. We also discuss results from a demonstration using an array over a longer 12.5 km baseline.

The Cassini and Kepler array demonstrations were found to validate the long term statistics acquired from several years of STI data as well as the models used to adjust the statistics for the conditions of an array. These statistics represent reliable estimates of the phase fluctuations that would be seen by an array tracking a deep space signal after applying appropriate adjustments for a given array configuration, elevation angle profile and observing frequency.

I. Introduction

Site test interferometers (STIs) that receive signals from geostationary satellites have been deployed at the three DSN tracking complexes for long-term monitoring of atmospheric delay fluctuations. These atmospheric delay fluctuations are statistically characterized seasonally (by month), annually and diurnally. Previous work describes the conditioning of these statistics and how they can be used to estimate array loss for prospective array configurations [1-2]. In a previous DSN array demonstration study involving the Cassini spacecraft, it was shown that statistics of the adjusted STI phase fluctuations matched the statistics of concurrent array demonstration phase fluctuations [3].

Since then, there have been several additional Ka-band array demonstrations, this time involving the Kepler spacecraft as summarized in Table 1. Table 1 describes each pass in terms of the Pass ID (as year-day number), the calendar date of the pass, the Deep Space Station (DSS) identifications involved in the array, and the span of the data used in UTC hours.

Table 1
Kepler Array Demonstration Passes

Pass ID	Date	DSS Stations	Data Span (UTC)
2014-316/317	Nov. 12-13, 2014	13/25 Goldstone	23:32 – 04:55
2015-192	July 11, 2015	25/26 Goldstone	00:50 – 01:00
2015-274	Oct. 01, 2015	25/26 Goldstone	21:54 – 23:55
2015-361	Dec. 27, 2015	25/26 Goldstone	01:52 – 05:00
2015-361	Dec. 27, 2015	54/55 Madrid	14:55 – 21:02

The carrier signal at 32.166 GHz emitted by the Kepler spacecraft was down-converted to baseband using in-phase (I) and quadrature-phase (Q) mixers driven by trajectory-based predictions of the carrier frequency. The signal was low-pass filtered and digitally sampled at 1 ksps at each station of the two-element array. The individual 1 ms samples from the recordings were pre-summed to output 0.1 s data points matching the sampling time of the STI signal data. In some cases, the array phase changed too quickly over a 0.1 s duration (causing ambiguities) and this necessitated using shorter intervals. The difference phase between the two arrayed elements, $\phi_{array}(t)$, was then processed and filtered as described in [3].

The STI data were processed as described in [3], with relevant detail repeated as follows. The received signal from each STI element (0.8 m antenna and outdoor electronics box) was downconverted to an Intermediate Frequency (IF) and then sent to a central processing rack in a temperature-controlled building. The IFs from each pair of elements were input to an IQ mixer board where the two signals were correlated and the resulting interferometric signal was captured in an output file in the form of I and Q components that were recorded every 0.1 s for each pair of elements.

During the post-processing, the phase time series estimated from the recorded I and Q samples was processed to remove cycle ambiguities. The resulting phase time series contained long-term contributions due to satellite motion and instrumental drift, as well as short-term atmospheric fluctuations and thermal noise. The slow changes were filtered out using 2nd degree polynomial fits over 10-minute blocks of data. The fitted model is subtracted from the phase data, and the resulting phase $\phi_{sti}(t)$ at the 0.1 s sample rate is dominated by short-term fluctuations due to atmosphere as supported by evidence provided in [3]. The short-term thermal noise is insignificant compared to the tropospheric fluctuations, except during very few instances where the troposphere was devoid of water vapor such as during the coldest winter night in the Goldstone, California desert climate.

To facilitate comparison of the STI measurements with those from the DSN array demonstration passes, the STI phases (or their statistics) are normalized or adjusted to conditions of the array. The line-of-sight phase measurements from the STI, $\phi_{sti}(t)$, are normalized to the conditions of the concurrent array observations by making adjustments for frequency, elevation angle, and antenna element spacing [3]. Equation (1) represents an estimate of the array phase, $\phi'_{array}(t)$, derived from the STI phase and the adjustments as shown below.

$$\phi'_{array}(t) = \phi_{sti}(t)\,\frac{f_{array}}{f_{sti}}\left(\frac{\sin(\theta_{sti})}{\sin\left(\theta_{array}(t)\right)}\right)^{\gamma}\left(\frac{r_{array}(t)}{r_{sti}}\right)^{\beta/2} \qquad (1)$$

where f_{sti}, θ_{sti}, and r_{sti}, are the measurement frequency, elevation angle, and projected baseline length against STI signal source, respectively, of the STI instrument; f_{array}, θ_{array}, and r_{array}, are the measurement frequency, elevation angle, and projected array baseline length against the array signal source (Kepler spacecraft), respectively, of the DSN array; and parameters γ, and β are discussed in the following text. The values for $r_{array}(t)$ and $\theta_{array}(t)$ are evaluated at each time sample using trajectory information obtained from [4-5]. We use a static value of f_{array} = 32.166 GHz in Eq. (1) for the spacecraft frequency since the relative changes due to Doppler are negligible over the pass. In (1), we have neglected the height adjustment term which is negligible given that the STI elements are located very close in height to the DSN array antennas, compared to the height of the turbulent layer. We provide in Table 2, the values for the relevant STI parameters used in equation (1) for Goldstone and Madrid. The value of r_{sti} represents the primary baseline of the data used in this study, (designated as baseline 1).

Table 2
STI Values used for adjustments

Case	f_{sti}, (GHz)	θ_{sti}, (deg)	r_{sti} (m)
Goldstone Baseline 1	12.45	47.03	191
Madrid Baseline 1	11.95	41.32	163

We assume that the troposphere is non-dispersive, thus the frequency adjustment in (1) is a straight-forward scaling, as there is insufficient water vapor in the atmosphere to cause any significant dispersion [1]. In addition, any fluctuations caused by the dispersive ionosphere lie well below those of the troposphere at the frequencies of interest [1].

The observed fluctuations will decrease with increase in elevation angle as air mass is inversely proportional to sin(θ). This dependence is linear (γ = 1 in Eq. (1)) if the turbulence along the signal path is dominated by a few large inhomogenities [6]. If the turbulence is dominated by many small, random inhomogenities, then their number along the signal path is proportional to air mass, and the effect on phase is proportional to the square root of that number (γ = 1/2) [6]. The general case lies between these two cases and has a complicated dependence on the geometry, which involves the thickness of the turbulent layer, H_w, as well as the average distance between the two signal paths, r, whereas the latter depends on the baseline length r as well as the azimuth and elevation angles of the signal paths [1]. In most cases, the signal path separation is taken to be the projected baseline length perpendicular to the signal path direction (r ~ 100 to 200 m). The height of the turbulent layer is typically 1 to 2 km [6], so usually $r << H_w$, which leads to $\gamma \approx ½$. In some cases H_w will be lower and γ will approach unity. For most analyses, we use γ = ½ for the thick screen model and γ = 1 for the thin screen model.

The adjustment for baseline length r in Eq. [1] depends on the three-dimensional spatial structure function of the refractive index. Using the Kolmogorov theory of turbulence and integrating vertically through the turbulent layer [6-7] gives the power law dependence in (1) with β = 5/3 when $r << H_w$ (thick screen) and β = 2/3 when $r >> H_w$ (thin screen). For this study, we used β = 5/3 for the thick screen model. In some cases, we used values of β derived from structure function fits from the STI data over the concurrent time interval of the array passes.

II. Goldstone Array Demonstrations - Cumulative distributions and statistics of phase time series

For array pass conducted on 2015-361 (December 27, 2015) involving Goldstone 34 m diameter antennas designated DSS-25 and DSS-26 (we use 25/26 hereafter to describe the array), we first examined a two hour period between 02:00 to 04:00 UTC of data. Concurrent STI data over same period were processed to extract interferometer phase over all three STI baselines. The STI phase data were adjusted for the conditions of the Kepler array (elevation angle, baseline projection, and frequency) using formulation in [3] and as shown in Eq. (1). The resulting phase residuals from the 25/26 array (red) and adjusted interferometer phase for STI baseline 1 (black) are shown in Figure 1 top panel for two successive time periods 02:00 – 03:00 UTC (left top), and (b) 03:00 – 04:00 UTC (right top). As can be seen in the respective plots in the bottom panel, the cumulative distribution of the array phase (red) agrees quite well with the cumulative distribution of the adjusted STI phase (black) for each interval. Similar results were observed with array demonstrations discussed in the previous study using the Cassini spacecraft [3].

If we calculate RMS scatter of the phase time series over 10-minutes intervals for the passes listed in Table 1, we can compare the array and adjusted STI phase scatter as shown in Figure 2. The RMS scatters for the short-baseline array and adjusted STI for each interval are within 30% of each other for the most part. Of the 64 10-minute segments shown in Figure 2, 49 of them have relative errors lying below 30% while 14 points lie above 30% with the highest value being 85%. The diagonal black line in Figure 2 displays the ideal model. We see that the data points for 2015-192 (25/26) (purple), 2015/361 (25/26) (red) and 2015-361 (54/55) (blue) lie close to or are reasonably distributed above and below the ideal curve. However, for pass 2015-274 (25/26) (yellow), almost all of the points lie above the ideal curve, suggesting that the array phase tends to exhibit more fluctuation than the adjusted STI phase. During the 2015-274 (25/26) pass, the array was tracking the Kepler spacecraft at low elevation angles (~20° to 30°) compared to the location of the geostationary satellite observed by the STI (47°), thus we may be seeing more (non-isotropic) turbulence along the array signal path. One does not

expect ideal or symmetric behavior as the atmosphere does not necessarily behave the same in all directions (not isotropic) and the signal paths of the array and STI are sampling different parts of the local atmosphere.

The cases involving the short (~300-m) baselines of 25/26 and 54/55 involve adjustments based on the thick layer model [3] as the lengths of both the STI baseline (~ 200 m) and DSN array (~ 300 m) are usually much smaller than the heights of the turbulent layer for Goldstone and Madrid. For reference, Figure 1 in [3] displays a satellite image showing the array and STI infrastructure at Goldstone for the short baseline array cases. The case of the longer 12.5 km baseline DSS-13/DSS-25 during 2014-316/317 to be discussed later made use of an alternate adjustment scheme.

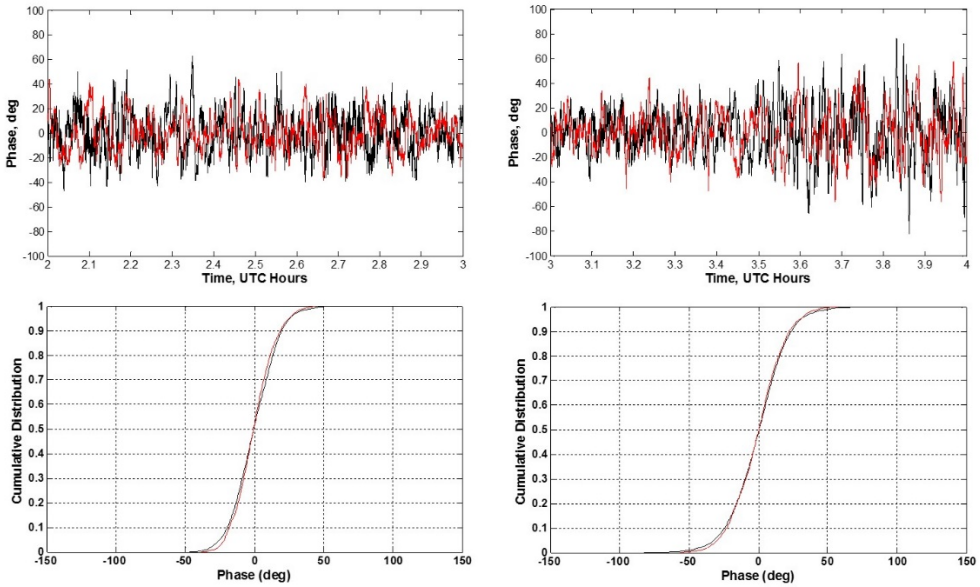

Figure 1 – Top Panel - Array phase (red) and adjusted STI phase (black) for two successive 1 h time periods from the 2015-361 (December 27, 2015) pass involving the 25/26 array. Bottom panel – Cumulative distribution for DSN array phase (red) and adjusted STI phase (black) for each of the time periods specified in the corresponding plots in the above panel.

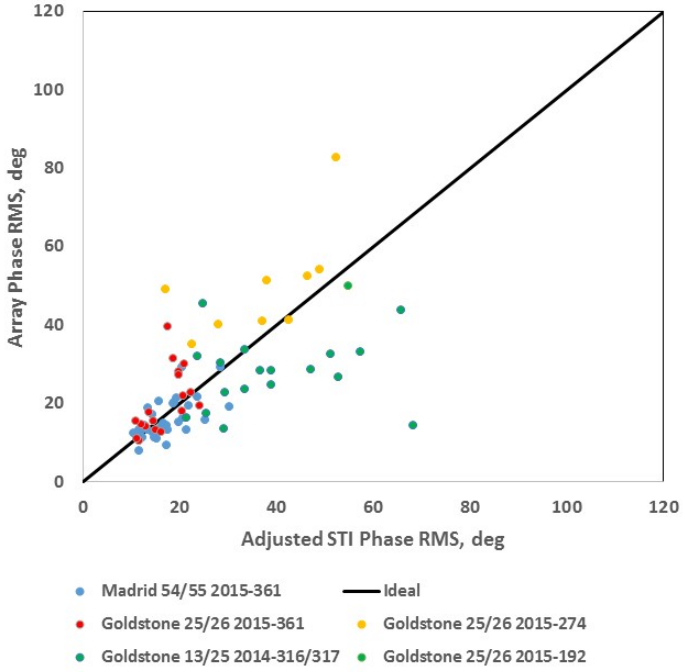

Figure 2 –Array phase RMS versus adjusted STI phase RMS over common 10-minute time periods. Diagonal black line shows ideal model.

III. Goldstone Array Demonstrations - Short time-scale features

For the array track on 2015-274 (October 1) between DSS-25 and DSS26, we examined 10-minute time periods of the phase data from 22:00 to 24:00 UTC. By examining the phase time series over shorter time periods, we can better discern detail between the array phase and adjusted STI phase. For example, Figures 3 and 4 display the phase time series for two different 10-minute time periods during 2015-274 (October 1, 2015) for the 25/26 array (red) and for the adjusted STI phase (black). Figure 3 illustrates the phase signatures for the period spanning from 22:50 to 23:00 UTC. Here we see periods of high correlation as well as periods with less correlation (or even anti-correlation such as at time 22.97 UTC). In any case, there are comparable levels of fluctuations between the phases of the two instruments when examining the respective cumulative distributions for this data set (not shown here). Figure 4 shows the phase behavior for the period between 23:30 to 23:40 UTC where there are again significant periods of correlation such as from 23.62 to 23.67 UTC. The Kepler signal path in the sky as seen by 25/26 array is near alignment with (within a few degrees) of the STI geostationary satellite signal path (STI azimuth = 201° elevation = 47°).

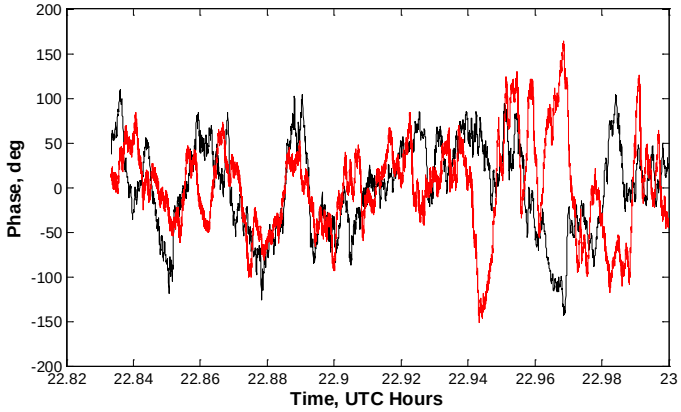

Figure 3 – Phase time series for 10-minute time interval from 22:50 to 23:00 UTC for 2015-274 (October 1, 2015) pass with 25/26 array (red) and adjusted STI phases (black).

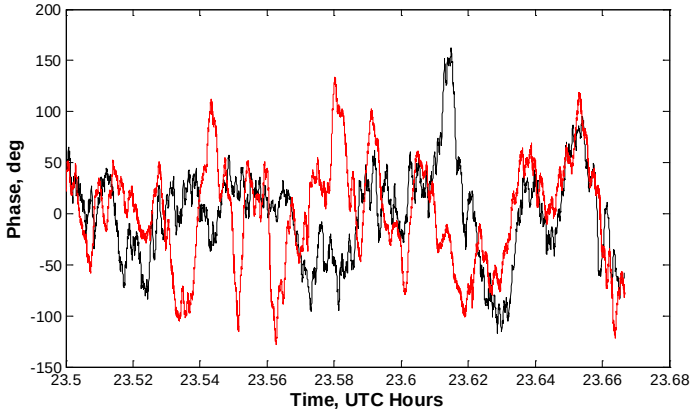

Figure 4 – Phase time series for 10-minute time interval from 23:30 to 23:40 UTC for 2015-274 (October 1, 2015) pass with 25/26 array (red) and adjusted STI phases (black).

Figure 5 displays the 25/26 array phase time series and adjusted STI phase time series for pass 2015-192 (July 11, 2015). For the data processing here, it was necessary to use shorter 5 s averaging sub-intervals for the array data. This is reflected in the visually evident larger short-term scatter of the array phase data (red curve in Figure 5). The STI data were adjusted for the conditions of the Kepler track in elevation angle, baseline projection, and sky frequency as described in Sec. I. The phase residuals from the 25/26 array (red) and adjusted STI (black) appear comparable with some differences. The resulting cumulative distributions of the phases for both time series were comparable.

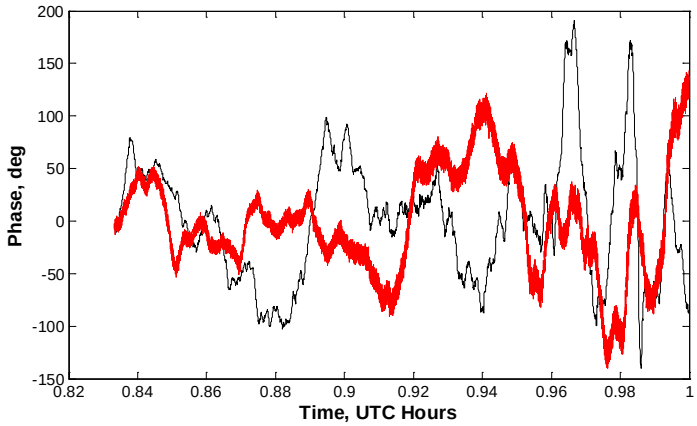

Figure 5 - Phase time series for 10-minute time interval from 00:50 to 01:00 UTC for 2015-192 (July 11, 2015) pass with 25/26 array (red) and adjusted STI (black).

IV. Goldstone Array Demonstrations - Thin Layer Case (DSS-13 and DSS-25)

A Kepler array demonstration pass was conducted on 2014-316/317 using a long 12.5 km baseline array (between DSS-13 and DSS-25) to exercise equipment in preparation for later array passes involving DSS-25 and DSS-26. This pass also provided an opportunity to test out thin-layer turbulence model assumptions. DSS-25 is situated in the Apollo valley where the STI resides and DSS-13, a Research and Development (R&D) antenna, is located 12.5 km away from the Apollo valley (see Figure 6). The length of this baseline is several times larger than the typical 1 km to 3 km height of the atmospheric turbulent layer thus allowing exploration of thin-layer turbulence model adjustments [3]. However, one expects that the atmospheric columns towards the spacecraft signal source are basically decorrelated over this distance, thus one does not expect to observe as many periods of correlation as seen with the shorter baseline (25/26 or 54/55) passes in the adjusted STI phase time series. However, the atmospheric conditions are expected to be sufficiently similar over the same climatic region such that the statistics of the observed phase fluctuations should be in reasonable agreement when the atmosphere is devoid of very turbulent conditions such as with the presence of large dense cells transiting the raypath over one station and not so much as the other station of the array.

Figure 6 – Terrain image map of the Goldstone complex showing the relative locations of the Apollo site (where DSS-25 and STI reside) and the Venus site (where DSS-13 resides). (Credit: Google Earth).

The Apollo east-west STI baseline data were adjusted to the conditions of the Kepler track. Figure 7a (left) shows 13/25 array phases along with STI phases adjusted (using Eq. (1)) only in frequency and elevation angle (thin layer adjustments). We note that the 12.5 km array phase residuals show significantly larger fluctuations than those of the partially adjusted 190 m STI. If we then further adjust the STI phases to match the projection of the array baseline (using the thin layer turbulence model with r_{sti} = 12.5 km in Eq. (1)), the levels of the array phase time series and the STI phase time

series more closely match (see Figure 7b). However, we see somewhat larger excursions for the adjusted STI data. If we examine the RMS phase data over all valid 10 min segments over the pass, almost all of the adjusted STI values exceed the corresponding array values. We then examined an alternative adjustment method where we used the height of the turbulent layer (r_{sti} = 2 km) in Eq. (1) for the array reaching the limit of the turbulence in its region along with intermediate values of the adjustment parameters (γ = 0.75, β = 1.0). Upon inspecting the resulting RMS values in each 10 min segment for this pass (green circles in Figure 2), we do see that some of them now lie above the ideal curve. However, most still lie below the ideal curve, suggesting that additional analysis and work is required. There is however reasonable agreement between the array and adjusted STI phase for several of the intervals. This may be indicative of the thin layer model assumptions breaking down or not being fully valid over such a long distance, as one also expects to see much smaller levels of correlation over this distance.

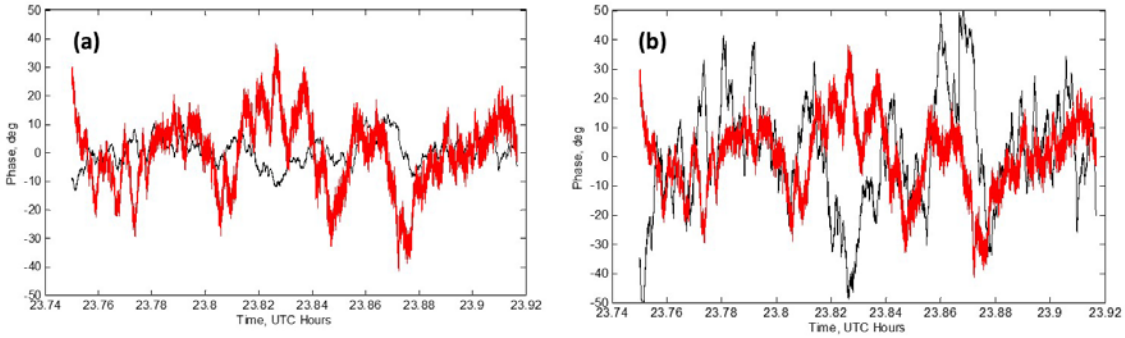

Figure 7 - (a) Shows 13/25 array phases (red) along with STI phase time series (black) adjusted only in frequency (32.166 GHz), and elevation angle. (b) Same as (a) except STI phases also adjusted to match the projection of the array baseline.

V. Madrid Array Demonstration – 2015-361 with 54/55

The Kepler Ka-band array demonstration pass performed on December 27, 2015 (2015-361) between the two Ka-band downlink capable 34 m antennas DSS-54 and DSS-55 in Madrid, Spain is discussed here. What makes this pass so interesting is that there is a portion where the line-of-sight to the Kepler spacecraft as viewed by the 54/55 array is about only about a degree away from the line-of-sight of the geostationary satellite as viewed by the Madrid STI. In addition, elements 2 and 3 of one of the STI baselines are each located next to DSS-54 and DSS-55, respectively, as shown in the satellite image of the Madrid site in Figure 8.

The results for this array demonstration show a very high degree of correlation between the STI baseline involving STI elements 2 and 3 adjusted phase time series and the 54/55 array phase time series as shown in Figure 9 for a given 10-minute interval. The cumulative distribution for each of the two phase time series (not shown) lie on top of each other. We do not expect perfect alignment of the two phase time series due to various such as the STI elements not being perfectly co-aligned with the BWG antennas (they are offset a few meters from each element), and there is a small ~ 1 deg offset between the two signal paths in the sky. In any event, this is a very encouraging result as it provides evidence that the models used in the adjustments are valid. A similar result was obtained for the baseline involving STI elements 1 and 2 (see Figure 8). However, there was less correlation with the baseline involving elements 1 and 3, which lies nearly perpendicular to the baseline coinciding with 54/55 (see Figure 8). We have seen periods of high correlation with passes involving the Goldstone 25/26 array (see Figures 3-4) but nothing with this degree of agreement. The closest the two line-of-sight signal paths between STI and array got during any of the Goldstone array demonstrations was about 4° [3].

For adjacent 10-minute intervals, we see the same basic correlation signatures of higher RMS phase scatters for the array than that for the STI. As the two line-of-sight signal paths diverge, we see less correlation in the phase signatures but have general agreement in RMS statistics within 10-minute segments (see blue circles in Figure 2).

From Figure 9, it is apparent that the slow features are well matched between the two interferometers, but not so much for the fast features. The slow features correspond to large-scale irregularities in the turbulent flow as they are carried over the antennas by the winds aloft, whereas the fast features correspond to smaller-scale irregularities. Although the STI antennas are adjacent to the DSN antennas, they are not coincident as they are separated by ~21-35 m. When looking in the same

direction, the signal paths are parallel but they are ~21-35 m apart as they traverse the lower atmosphere. Thus, both instruments would sense the same large-scale features but different small-scale features. The wind near the surface during this 10 min period was variable with wind speeds ranging from 4.9 to 14.2 km/h and wind directions ranging from 38° to 86° (based on local weather tower data). The range of delay discerned from the array and adjusted STI phase features (see Figure 9) is consistent with the range of delay inferred from the wind speeds and element offsets.

Figure 8 – Layout of Madrid site showing locations of the three STI elements (1, 2 and 3) as well as the locations of the 34-m diameter antennas, DSS-54 and DSS-55. (Credit: Google Earth).

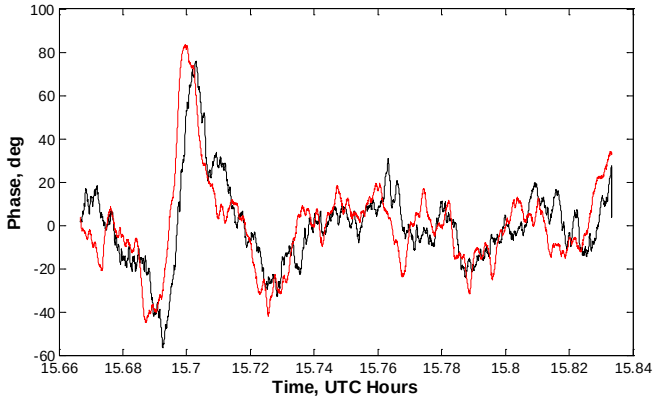

Figure 9 – Madrid DSS-54 and DSS-55 array phase time series (red) and adjusted STI phase time series (black) for segment of pass 2015-361 occurring between 15:40 and 15:50 UTC.

Acknowledgements: We thank Danny Kahan of the radio science support team for his assistance in preparing and delivering the open-loop receiver data sets used in this study; DSN operations and the Kepler project for their cooperation; and Peter Kinman for valuable review comments. The research was carried out at the Jet Propulsion Laboratory, California Institute of Technology, under a contract with the National Aeronautics and Space Administration.

References:

[1] Morabito, D. D., L. R. D'Addario, R. J. Acosta, and J. A. Nessel (2013), Tropospheric delay statistics measured by two site test interferometers at Goldstone, California, Radio Sci., 48, doi:10.1002/2013RS005268. http://onlinelibrary.wiley.com/doi/10.1002/2013RS005268/abstract

[2] Morabito, D. D. and L. R. D'Addario, "Atmospheric Array Loss Statistics for the Goldstone and Canberra DSN Sites Derived from Site Test Interferometer Data," IPN PR 42-196, pp. 1-23, February 15, 2014.

[3] Morabito, D. D., L. D'Addario, and S. Finley (2016), A comparison of atmospheric effects on differential phase for a two-element antenna array and nearby site test interferometer, Radio Sci., 51, doi:10.1002/2015RS005763.

[4] Giorgini JD, Yeomans DK, Chamberlin AB, Chodas PW, Jacobson RA, Keesey MS, Lieske JH, Ostro SJ, Standish EM, Wimberly RN, "JPL's On-Line Solar System Data Service", BULLETIN OF THE AMERICAN ASTRONOMICAL SOCIETY, Vol 28, No. 3, p. 1158, 1996.

[5] Giorgini, JD and JPL Solar System Dynamics Group, "NASA/JPL Horizons On-Line Ephemeris System," http://ssd.jpl.nasa.gov/?horizons, data retrieved 2014-Sep-30.

[6] Treuhaft, R. N., and G. E. Lanyi (1987), The effect of the dynamic wet-troposphere on radio interferometric measurements, Radio Sci., vol. 22, No. 2, pp. 251-265, Mar.-Apr. 1987.

[7] Coulman, C. (1985), Fundamental and applied aspects of astronomical seeing, Ann. Rev. of Astron. and Astrophys., vol. 23, pp. 19-57, 1985.